

System-size convergence of nonthermal particle acceleration in relativistic plasma turbulence

VLADIMIR ZHDANKIN,¹ DMITRI A. UZDENSKY,² GREGORY R. WERNER,² AND MITCHELL C. BEGELMAN^{1,3}

¹*JILA, NIST and University of Colorado, 440 UCB, Boulder, Colorado 80309, USA*

²*Center for Integrated Plasma Studies, Department of Physics, 390 UCB, University of Colorado, Boulder, CO 80309, USA*

³*Department of Astrophysical and Planetary Sciences, 391 UCB, Boulder, CO 80309, USA*

(Received May 23, 2018; Revised May 23, 2018; Accepted May 23, 2018)

Submitted to ApJ

ABSTRACT

We apply collisionless particle-in-cell simulations of relativistic pair plasmas to explore whether driven turbulence is a viable high-energy astrophysical particle accelerator. We characterize nonthermal particle distributions for varying system sizes up to $L/2\pi\rho_{e0} = 163$, where $L/2\pi$ is the driving scale and ρ_{e0} is the initial characteristic Larmor radius. We show that turbulent particle acceleration produces power-law energy distributions that, when compared at a fixed number of large-scale dynamical times, slowly steepen with increasing system size. We demonstrate, however, that convergence is obtained by comparing the distributions at different times that increase with system size (approximately logarithmically). We suggest that the system-size dependence arises from the time required for particles to reach the highest accessible energies via Fermi acceleration. The converged power-law index of the energy distribution, $\alpha \approx 3.0$ for magnetization $\sigma = 3/8$, makes turbulence a possible explanation for nonthermal spectra observed in systems such as the Crab nebula.

Keywords: acceleration of particles, magnetohydrodynamics (MHD), plasmas, pulsars: individual (Crab), relativistic processes, turbulence

1. INTRODUCTION

For many decades, turbulence has been recognized as a conceivable source of nonthermal energetic particles in collisionless plasmas. Theoretical works have proposed a variety of routes toward particle acceleration, including diffusive (second-order) acceleration from turbulent fluctuations [Alfvénic modes (Jokipii 1966; Schlickeiser 1989; Chandran 2000; Cho & Lazarian 2006); compressive modes (Schlickeiser & Miller 1998; Yan & Lazarian 2002; Chandran 2003); kinetic modes (e.g., Dermer et al. 1996; Fonseca et al. 2003; Petrosian & Liu 2004; Riquelme et al. 2017)] and secular (first-order) acceleration via intermittent structures [shocks (Bykov & Topogin 1982; Blandford & Eichler 1987); current sheets undergoing magnetic reconnection (Vlahos et al. 2004; Lazarian et al. 2012; Isliker et al. 2017); see also Beresnyak & Li (2016)]. These mechanisms of acceleration

are tantalizing theoretical possibilities, but rely on various assumptions about the nature of turbulence and nonlinear plasma physics. Due the complexity and analytic intractability of the problem, the only practical way to prove the reality of turbulent particle acceleration (apart from direct experimental confirmation) is with self-consistent, large-scale numerical simulations.

Turbulent particle acceleration has important implications for space systems such as the solar corona, the solar wind, and planetary magnetospheres, as well as for high-energy astrophysical systems such as pulsar wind nebulae, X-ray binaries, supernovae remnants, jets from active galactic nuclei (including blazars), radio lobes, and gamma ray bursts. Observations of broadband radiation spectra and cosmic rays imply that nonthermal particles are a significant component of the universe. In this work, we focus on plasmas that are relativistically hot with modestly relativistic bulk velocities, as found in many high-energy astrophysical settings.

In our previous work (Zhdankin et al. 2017), we applied particle-in-cell (PIC) simulations to demonstrate that driven turbulence can produce a substantial pop-

ulation of nonthermal particles in relativistic pair plasmas, with power-law energy distributions that become harder with increasing magnetization (ratio of magnetic enthalpy to relativistic plasma enthalpy). However, these simulations also revealed that the distributions became softer with increasing system size, and were therefore unable to probe distributions in the asymptotic large-system limit. In principle, a lack of convergence can arise from inadequate scale separation, or from the adverse role of physical effects such as scale-dependent anisotropy, intermittency, damping of relevant (e.g., compressive) modes, or the inherent inefficiency of the acceleration process at magnetohydrodynamic (MHD) scales. Since supercomputers will be unable to simulate systems with sizes comparable to real astrophysical systems in the foreseeable future, it is necessary to understand the scaling of nonthermal particle distributions with system size before applying such simulations to model astrophysical phenomena.

In the present work, we address the system-size dependence of turbulent particle acceleration. We confirm a weak system size dependence for nonthermal energy distributions when measured at a fixed number of large-scale dynamical times, for sizes extending beyond those considered in Zhdankin et al. (2017). However, more importantly, we present evidence that the distributions converge when compared at different times that increase with system size (approximately logarithmically or as a weak power law). Physically, this time dependence arises from the fact that the distributions do not fully develop until particles reach the highest accessible energies via Fermi acceleration. The converged value of the index for the power-law energy distribution ($\alpha \approx 3.0$ for magnetization $\sigma = 3/8$) confirms turbulence as an efficient, viable astrophysical particle accelerator.

2. SIMULATIONS

We perform the simulations with the explicit electromagnetic PIC code ZELTRON (Cerutti et al. 2013) using charge-conserving current deposition (Esirkepov 2001). The simulation set-up is described in detail in Zhdankin et al. (2018); here, we simply outline the main features. The domain is a periodic cubic box of size L^3 (consisting of N^3 cells) with uniform mean magnetic field $\mathbf{B}_0 = B_0 \hat{z}$. We initialize electrons and positrons from a uniform Maxwell-Jüttner distribution with combined particle density n_0 and temperature $T_0 = \theta_0 mc^2$, where m is the electron rest mass, and we choose $\theta_0 = 100$ (giving an ultra-relativistic initial mean Lorentz factor of $\gamma_0 \approx 300$). We then drive strong ($\delta B_{\text{rms}} \sim B_0$) turbulence at low wavenumber modes ($k = 2\pi/L$) by applying a randomly fluctuating external current den-

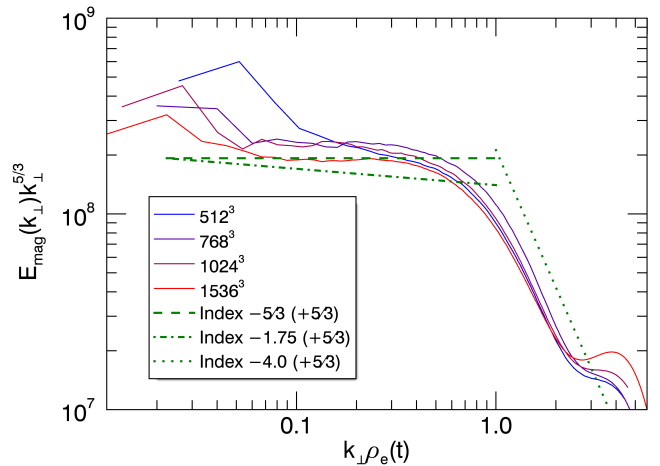


Figure 1. Magnetic energy spectrum compensated by $k_{\perp}^{5/3}$ for varying system sizes. Power laws with pre-compensated indices of $-5/3$ (dashed), -1.75 (dash-dotted), and -4 (dotted) are shown for reference.

sity (TenBarge et al. 2014). For these simulations, we fix the initial magnetization to $\sigma_0 \equiv B_0^2/4\pi h_0 = 3/8$, where $h_0 = 4n_0\theta_0 mc^2$ is the initial relativistic enthalpy density. The initial Alfvén velocity is given by $v_{A0} \equiv c[\sigma_0/(\sigma_0 + 1)]^{1/2} \approx 0.52c$; we perform each simulation for a duration of at least $7.5L/v_{A0}$. As optimized by convergence studies, we set the initial Larmor radius to $\rho_{e0} \equiv \gamma_0 mc^2/eB_0 = 1.5\Delta x$ (where Δx is the cell size) and choose 64 particles per cell for the main simulations.

We perform a scan over system size $L/2\pi\rho_{e0}$ by varying the number of cells in each simulation, taking $N \in \{256, 384, 512, 768, 1024, 1536\}$, so that $L/2\pi\rho_{e0} \in \{27.2, 40.7, 54.3, 81.5, 109, 163\}$. To check reproducibility, we reran all of the cases having $N \leq 1024$ with a different random seed (for particle initialization and driving phases); for robustness, we analyze the particle distributions averaged for each simulation pair at a given size. We also perform statistical ensembles of sixteen 384^3 cases and eight 768^3 cases with 32 particles per cell to investigate statistical variation of the results.

3. RESULTS

The time evolution of the simulations proceeds as discussed in our previous papers (Zhdankin et al. 2017; Zhdankin et al. 2018): the external driving disrupts the initial thermal equilibrium and establishes turbulent fluctuations across a broad range of scales. The turbulence is fully developed after a few Alfvén times, after which turbulent energy dissipation increases the internal energy at a constant rate. For reference, in Fig. 1, we show the magnetic energy spectrum compensated by $k_{\perp}^{5/3}$, where k_{\perp} is the wavenumber perpendicular to \mathbf{B}_0 , for simulations of varying size, averaged over 5 snap-

shots from $3.1 \leq tv_{A0}/L \leq 5.2$. Whereas the 512^3 case has a spectrum that is steeper than $k_{\perp}^{-5/3}$, the larger cases (768^3 and above) have spectra close to $k_{\perp}^{-5/3}$, in agreement with classical MHD turbulence theories (Goldreich & Sridhar 1995; Thompson & Blaes 1998). The 1536^3 case exhibits an inertial range from $k_{\perp}\rho_e \sim 0.06$ to $k_{\perp}\rho_e \sim 0.4$, where $\rho_e = \langle \gamma \rangle mc^2 / eB_{\text{rms}}$ is the characteristic Larmor radius based on the instantaneous mean particle Lorentz factor $\langle \gamma \rangle$.

We now turn to the particle energy distribution $f(\gamma)$, where the particle Lorentz factor $\gamma = E/mc^2$ is used interchangeably with energy E . The evolution of $f(\gamma)$ for the 1536^3 simulation is shown in the top panel of Fig. 2. As in our previous work (Zhdankin et al. 2017), the distribution develops a power-law tail, $f(\gamma) \sim \gamma^{-\alpha}$, over several dynamical times, attaining an index of $\alpha \approx 3.0$ at $tv_{A0}/L \sim 7$. This power law extends from energies comparable to the instantaneous mean ($\langle \gamma \rangle \sim 1.5 \times 10^3$) up to energies limited by the system size ($\gamma_{\text{max}} \equiv LeB_0/2mc^2 \sim 1.5 \times 10^5$), extending across a factor of ~ 50 in energy. At later times (not shown), particles accumulate at energies near γ_{max} , causing a high-energy pileup in the distribution.

In the middle panel of Fig. 2, we show the energy distributions at a fixed number of large-scale dynamical times, taken to be $tv_{A0}/L = 7.0$, for simulations of varying size (512^3 to 1536^3). For clarity, we compensate the distributions by γ^3 , making the 1536^3 case horizontal. The nonthermal tail steepens with increasing system size, ranging from an estimated index of $\alpha \approx 2.7$ for the 512^3 case to $\alpha \approx 3.0$ for the 1536^3 case. Thus, when compared at fixed times, there is no clear evidence for convergence of $f(\gamma)$ with system size; although the scaling of α with size is weak ($\delta\alpha \sim 0.3$ for a factor of 3 increase in size), it can undermine the viability of turbulent particle acceleration in astrophysical systems if it persists to larger sizes.

The interpretation of the data changes, however, when the energy distributions are compared at different times, chosen to scale with system size. In the bottom panel of Fig. 2, we show distributions at $tv_{A0}/L \in \{5.2, 5.8, 6.4, 7.0\}$ for the simulations with $\{512^3, 768^3, 1024^3, 1536^3\}$ cells (which is an approximately logarithmic increase of time with size). When compared at these times, the 768^3 , 1024^3 , and 1536^3 simulations all exhibit converged distributions with index near $\alpha \approx 3.0$, to within ± 0.1 accuracy. Notably, these times approximately coincide with the initial formation of the pileup at γ_{max} . This leads to our main proposal, that *turbulent particle acceleration produces a power-law particle energy distribution that converges with increasing system size, but the time required to*

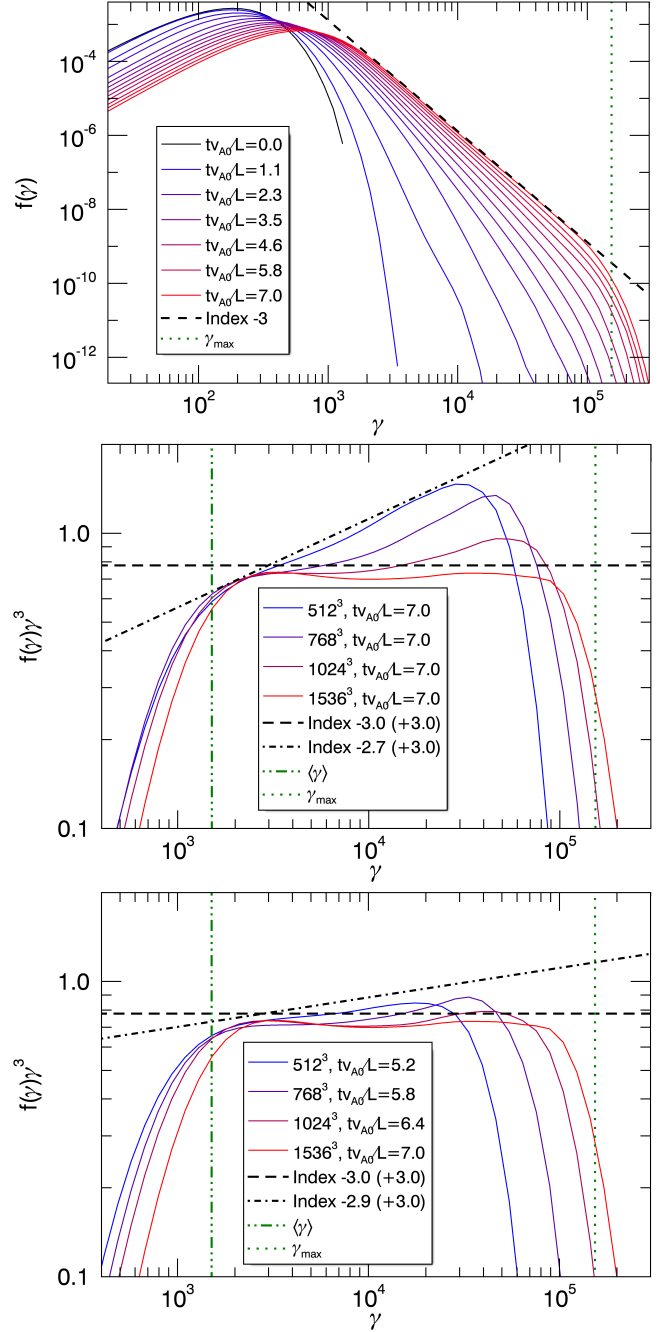


Figure 2. Top panel: Evolution of the particle energy distribution $f(\gamma)$ for the 1536^3 simulation. Center panel: Compensated distribution $f(\gamma)\gamma^3$, at fixed time $tv_{A0}/L = 7.0$, for varying system sizes. Power laws with pre-compensated index -3.0 (black dashed) and -2.7 (black dash-dotted) are also shown, along with the mean energy $\langle \gamma \rangle$ (green dash-dotted) and system-size cutoff γ_{max} (green dotted) for the 1536^3 case. Bottom panel: Similar compensated distributions at times increasing logarithmically with size. Power laws with pre-compensated index -3.0 (black dashed) and -2.9 (black dash-dotted) are shown in this case.

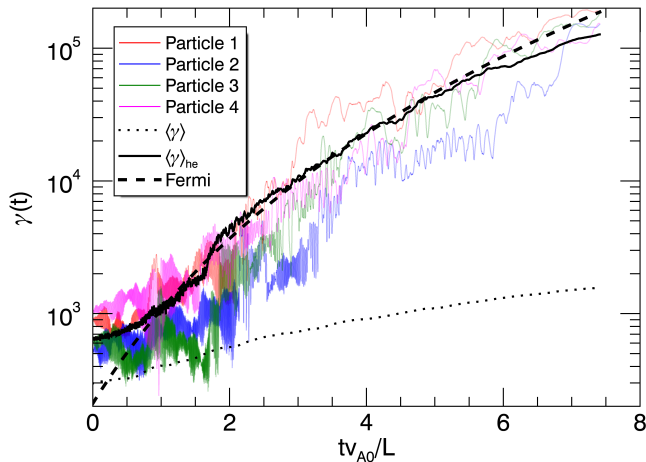


Figure 3. Energy evolution of four particles that attain the highest final energies in the tracked particle sample (solid, colored), along with average of particles that attain $\gamma > 10^5$ (solid, black). The prediction from second-order Fermi acceleration (Eq. 4; black, dashed) and the overall mean particle energy $\langle \gamma \rangle$ (black, dotted) are also shown for reference.

fully form this distribution slowly increases with system size. We suggest that the apparent size dependence of the (fixed-time) index α in our simulations is due to the power laws becoming contaminated by the pileup at γ_{\max} , which develops earlier for smaller systems. We now provide physical motivation for this proposal by considering the particle acceleration process in detail.

To understand the acceleration process, we tracked a random sample of 8×10^5 particles in each simulation. In Fig. 3, we show the energy evolution for the four tracked particles that attain the highest energies at the end of the 1536³ simulation. These four particles are the only tracked particles with final energies $\gamma > \gamma_{\max}$. At early times, the particle energies exhibit rapid oscillations on a timescale comparable to their Larmor period. The particles occasionally undergo acceleration episodes in which their energy rapidly increases by a factor of 2 or more, but the overall acceleration takes place gradually over several large-scale dynamical times.

In the same figure, we show the average energy evolution for all tracked particles with final energies $\gamma > 10^5$ (yielding 44 particles), denoted $\langle \gamma \rangle_{\text{he}}$. After turbulence is fully developed, $\langle \gamma \rangle_{\text{he}}$ increases at a slightly sub-exponential rate, until it approaches γ_{\max} . As we now show, this energy evolution is consistent with Fermi acceleration with a slowly evolving acceleration timescale. We suppose that the scattering process causes particle energies to increase as

$$\frac{d\gamma}{dt} \sim \frac{\gamma}{\tau_{\text{acc}}}, \quad (1)$$

where $\tau_{\text{acc}}(t)$ is the acceleration timescale. For second-order Fermi acceleration, assuming scattering by large-scale fluctuations, the acceleration timescale is

$$\tau_{\text{acc}} \sim \frac{3}{4} \frac{\lambda_{\text{mfp}} c}{u_A^2}, \quad (2)$$

where $u_A = v_A / (1 - v_A^2/c^2)^{1/2} = \sigma^{1/2} c$ is the Alfvén four-velocity and λ_{mfp} is the scattering mean free path (Longair 2011). For time-independent τ_{acc} , Eq. 1 leads to an exponential increase in the particle energy. The time required for particles to reach γ_{\max} from an initial energy of $\gamma_i \sim \gamma_0$ is then $t/\tau_{\text{acc}} \sim \log(\gamma_{\max}/\gamma_i) \sim \log(L/\rho_{e0})$. In relativistic plasmas with no energy sink, however, the acceleration timescale evolves with time since the Alfvén velocity decreases due to turbulent energy dissipation increasing the relativistic plasma inertia. As discussed in Zhdankin et al. (2018), for a constant energy injection rate, $\langle \gamma \rangle \sim \gamma_0(1 + \eta\sigma_0 v_{A0} t/L)$ (where $\eta \approx 1$ is the measured injection efficiency for the given simulations), the Alfvén velocity $v_A(t)$ is given by

$$\begin{aligned} \frac{v_A}{c} &= \sqrt{\frac{\sigma}{\sigma + 1}} = \left(1 + \frac{\langle \gamma \rangle}{\sigma_0 \gamma_0}\right)^{-1/2} \\ &\sim \frac{v_{A0}}{c} \left(1 + \eta \frac{v_{A0}^2}{c^2} \frac{tv_{A0}}{L}\right)^{-1/2}. \end{aligned} \quad (3)$$

The energy growth due to second-order Fermi acceleration is then a power law in time (solving Eqs. 1-3),

$$\gamma \sim \gamma_i \left(1 + \eta\sigma_0 \frac{tv_{A0}}{L}\right)^{4Lc/3\eta\lambda_{\text{mfp}}v_{A0}}. \quad (4)$$

Note that, using the identity $(1 + x/n)^n \rightarrow \exp x$ as $n \rightarrow \infty$, this equation approaches an exponential in the limit of $\eta\sigma_0 \ll 1$, consistent with time-independent Fermi acceleration. We find that Eq. 4 provides a good fit to $\langle \gamma \rangle_{\text{he}}$, as shown in Fig. 3, if we take $\lambda_{\text{mfp}}/L = 1/2$ and $\gamma_i = 0.7\gamma_0$ (giving $\gamma \propto t^{5.1}$ at late times). These results imply that the second-order Fermi process can account for particle acceleration observed in the simulations. First-order acceleration may also contribute; measuring the relative importance of first-order and second-order mechanisms is left for future work.

Inverting Eq. 4 gives the time required for the particle to reach a given energy γ ,

$$\frac{tv_{A0}}{L} \sim \frac{1}{\eta\sigma_0} \left[\left(\frac{\gamma}{\gamma_i}\right)^{3\eta\lambda_{\text{mfp}}v_{A0}/4Lc} - 1 \right]. \quad (5)$$

This equation can be used to estimate the time required for Fermi-accelerated particles to reach the system size limit ($\gamma \sim \gamma_{\max}$). Note that Eq. 5 approaches a logarithmic function in the limit of $\eta\sigma_0 \ll 1$.

We now relate Fermi acceleration to the late-time evolution of the energy distributions. As previously discussed, the distributions form a power law and then subsequently develop a broad pileup near γ_{\max} . It is natural to focus on the distribution just prior to the pileup formation, when the power law has its maximum extent. After the power law is fully formed, a pair of inflection points appear due to the pileup (which makes the distribution no longer concave down). We define the inflection time, t_{inf} , as the latest time at which the difference between local power-law indices [$\alpha(\gamma) \equiv -\partial \log f / \partial \log \gamma$] at the two inflection points [local extrema of $\alpha(\gamma)$] is less than 0.1. For $t > t_{\text{inf}}$, the distributions become influenced by the pileup, making a power-law index difficult to define precisely.

The normalized inflection time $t_{\text{inf}} v_{A0} / L$ versus system size $L / 2\pi\rho_{e0}$ is shown in the top panel of Fig. 4. We find that $t_{\text{inf}} v_{A0} / L$ increases with size, consistent with particles requiring a longer number of larger-scale dynamical times to reach γ_{\max} . In fact, t_{inf} is consistent with the second-order Fermi acceleration timescale calculated in Eq. 5 [with $L_{\text{mfp}} / L = 1/2$ and $\gamma_i = \gamma_0$, giving $t_{\text{inf}} \propto (\gamma_{\max} / \gamma_0)^{0.2}$], which is also shown the top panel of Fig. 4. This scaling is close to logarithmic over the given range of sizes. We note that the time taken for the distribution to reach energies slightly beyond γ_{\max} exhibits a similar scaling as for t_{inf} (not shown). The system-size dependence of the inflection time, and related pileup, gives a motivation for comparing $f(\gamma)$ at times that increase according to Eq. 5.

In the bottom panel of Fig. 4, we show the index α (measured at the logarithmic center of the power law segment) versus system size $L / 2\pi\rho_{e0}$ taken at various times: the inflection time $t = t_{\text{inf}}$, logarithmic times $t \propto \log(L / 2\pi\rho_{e0})$, arbitrary fixed time $t = 7L / v_{A0}$, and at times with fixed mean particle energy $\langle \gamma \rangle \sim 4.2\gamma_0$ (which is nominally the same as fixed time, but sensitive to statistical variations). We find that measuring the distribution at fixed time or fixed injected energy shows a clear system size dependence, although the dependence weakens with size; in particular, α exhibits an approximately logarithmic dependence on $L / 2\pi\rho_{e0}$ [somewhat weaker than suggested in (Zhdankin et al. 2017)]. In contrast, the distribution taken at the inflection time or at logarithmic times shows no systematic variation for $L / 2\pi\rho_{e0} \gtrsim 80$. The sum up, distributions attain the same power-law index, independent of system size, just prior to pileup formation.

We conclude with a comment about the statistical significance of our results. In our simulations, the amount of energy injected into the plasma by the external driving fluctuates randomly in time, since driven mode

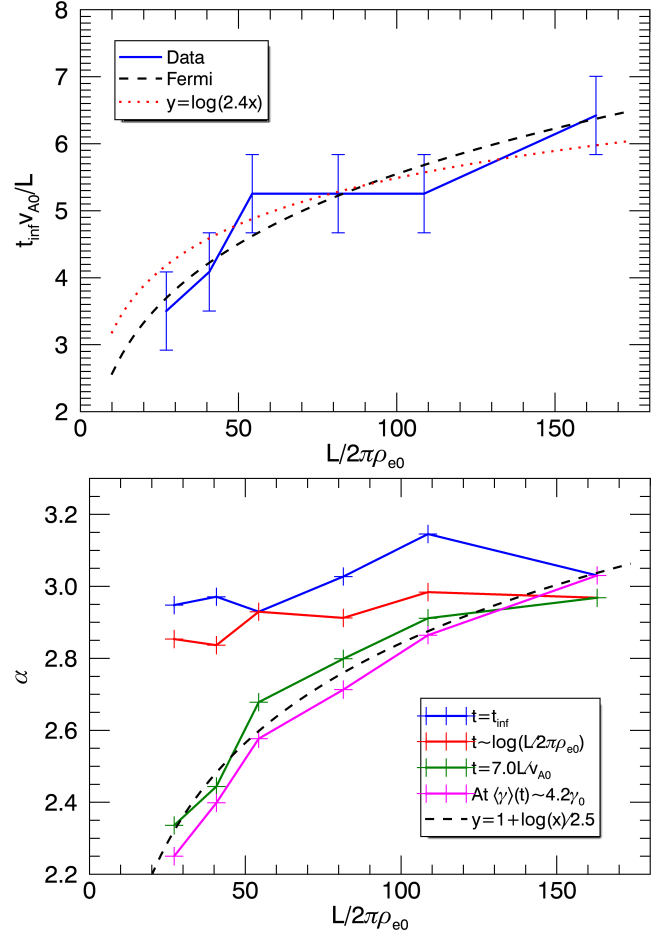


Figure 4. Top panel: Time taken for the primary inflection point to appear in the energy distribution, t_{inf} , versus system size $L / 2\pi\rho_{e0}$. The predicted time for particles to be Fermi-accelerated to the system-size limit γ_{\max} (Eq. 5; black, dashed) and a logarithmic scaling (red, dotted) are also shown. Error bars indicate the time intervals between successive measurements of the distribution. Bottom panel: Power-law index α vs $L / 2\pi\rho_{e0}$ measured at various times: at the inflection time t_{inf} (blue), at times scaling logarithmically with size (red), at arbitrary fixed time $t = 7L / v_{A0}$ (green), and at times with fixed mean particle energy, $\langle \gamma \rangle \sim 4.2\gamma_0$ (magenta). A logarithmic fit is shown for comparison (black, dashed).

phases are evolved randomly. While the mean energy injection rate approaches a universal value for sufficiently long simulations, the distributions presented in this paper were measured after a limited duration ($\lesssim 7L / v_{A0}$) and thus the amount of injected energy at that point can vary significantly between different runs (by up to $\sim 30\%$). In principle, a larger injection of energy may supply a harder nonthermal population, bringing up an important question: do the measured nonthermal distributions exhibit significant statistical variability (from run to run) due to random driving? To build confidence

that our largest simulations are not statistical outliers, we analyzed ensembles of sixteen 384^3 ($L/2\pi\rho_{e0} = 40.7$) and eight 768^3 ($L/2\pi\rho_{e0} = 81.5$) simulations. For the 384^3 ensemble, we obtain an average fixed-time index of $\langle\alpha\rangle \approx 2.53$ and rms spread of $\delta\alpha_{\text{rms}} \approx 0.06$ (at $t = 7L/v_{A0}$), with α weakly correlated with injected energy. For the 768^3 ensemble, we find $\langle\alpha\rangle \approx 2.79$ and $\delta\alpha_{\text{rms}} \approx 0.07$, indicating that the statistical spread is similar at both sizes and is less than the difference due to size. When measured at logarithmic times, we find $\langle\alpha\rangle \approx 2.86$, $\delta\alpha_{\text{rms}} \approx 0.09$ for the 384^3 ensemble (at $tv_{A0}/L \approx 4.2$) and $\langle\alpha\rangle \approx 2.94$, $\delta\alpha_{\text{rms}} \approx 0.06$ for the 768^3 ensemble (at $tv_{A0}/L \approx 5.2$), in agreement with Fig. 4. In addition to this, we find that the variations are modest in each pair of equal-size simulations from our main system-size scan. Hence, we believe that trends measured in our simulations are robust.

4. CONCLUSIONS

Based on the simulations presented in this paper, we are prepared to declare the system-size independence of power-law indices of particle energy distributions produced by driven, large-scale turbulence in relativistic collisionless plasmas. We empirically observe that convergence of the power-law indices occurs at times that depend on system size (approximately logarithmically or as a weak power law). We propose a physical interpretation for this dependence of time on system size: as the size is increased, there is an increasing number of scatterings required for particles to acquire the highest accessible energies via Fermi acceleration. The energy distribution becomes fully developed only once particles reach the energy limit γ_{max} due to finite system size, and subsequently the distributions experience a high-energy pileup that may complicate measurements of the power law. This pile-up forms due to constant energy injection into a closed system, which is an unrealistic scenario; in general, particle energies may be limited by

other physics, such as radiative cooling or open boundaries.

This work demonstrates that accurately measuring the converged power-law index is feasible with modestly large PIC simulations of turbulence (with $L/2\pi\rho_e \gtrsim 80$). We find a converged index of $\alpha \approx 3.0$ at magnetization $\sigma = 3/8$ and turbulence amplitude $\delta B_{\text{rms}} \sim B_0$; as discussed in Zhdankin et al. (2017), turbulent particle acceleration becomes more efficient with increasing σ , leading to smaller values of α and faster formation of the nonthermal population (as implied by Eq. 5). A similar converged value of the index, for comparable plasma parameters, is measured in PIC simulations of relativistic magnetic reconnection (e.g., Werner & Uzdensky 2017); slightly steeper indices are measured for relaxation of magnetostatic equilibria (Nalewajko et al. 2016). Likewise, our measured index is very close to the index of ≈ 3.2 inferred from the continuum synchrotron spectrum in the Crab nebula, where a magnetization below unity is expected (Meyer et al. 2010).

The authors acknowledge support from NSF grant AST-1411879 and NASA ATP grants NNX16AB28G and NNX17AK57G. An award of computer time was provided by the Innovative and Novel Computational Impact on Theory and Experiment (INCITE) program. This research used resources of the Argonne Leadership Computing Facility, which is a DOE Office of Science User Facility supported under Contract DE-AC02-06CH11357. This work also used the Extreme Science and Engineering Discovery Environment (XSEDE), which is supported by National Science Foundation grant number ACI-1548562. This work used the XSEDE supercomputer Stampede2 at the Texas Advanced Computer Center (TACC) through allocation TG-PHY160032 (Towns et al. 2014).

REFERENCES

- Beresnyak, A., & Li, H. 2016, *The Astrophysical Journal*, 819, 90
- Blandford, R., & Eichler, D. 1987, *Physics Reports*, 154, 1
- Bykov, A., & Toptygin, I. 1982, *Journal of Geophysics Zeitschrift Geophysik*, 50, 221
- Cerutti, B., Werner, G. R., Uzdensky, D. A., & Begelman, M. C. 2013, *The Astrophysical Journal*, 770, 147
- Chandran, B. D. 2000, *Physical Review Letters*, 85, 4656
- . 2003, *The Astrophysical Journal*, 599, 1426
- Cho, J., & Lazarian, A. 2006, *The Astrophysical Journal*, 638, 811
- Dermer, C. D., Miller, J. A., & Li, H. 1996, *The Astrophysical Journal*, 456, 106
- Esirkepov, T. Z. 2001, *Computer Physics Communications*, 135, 144
- Fonseca, R. A., Silva, L. O., Tonge, J. W., Mori, W. B., & Dawson, J. M. 2003, *Physics of Plasmas*, 10, 1979
- Goldreich, P., & Sridhar, S. 1995, *The Astrophysical Journal*, 438, 763
- Islaker, H., Vlahos, L., & Constantinescu, D. 2017, *Physical Review Letters*, 119, 045101
- Jokipii, J. R. 1966, *The Astrophysical Journal*, 146, 480

- Lazarian, A., Vlahos, L., Kowal, G., et al. 2012, Space science reviews, 173, 557
- Longair, M. S. 2011, High energy astrophysics (cambridge university Press)
- Meyer, M., Horns, D., & Zechlin, H.-S. 2010, Astronomy & Astrophysics, 523, A2
- Nalewajko, K., Zrake, J., Yuan, Y., East, W. E., & Blandford, R. D. 2016, The Astrophysical Journal, 826, 115
- Petrosian, V., & Liu, S. 2004, The Astrophysical Journal, 610, 550
- Riquelme, M., Osorio, A., & Quataert, E. 2017, The Astrophysical Journal, 850, 113
- Schlickeiser, R. 1989, The Astrophysical Journal, 336, 243
- Schlickeiser, R., & Miller, J. A. 1998, The Astrophysical Journal, 492, 352
- TenBarge, J., Howes, G. G., Dorland, W., & Hammett, G. W. 2014, Computer Physics Communications, 185, 578
- Thompson, C., & Blaes, O. 1998, Physical Review D, 57, 3219
- Towns, J., Cockerill, T., Dahan, M., et al. 2014, Computing in Science & Engineering, 16, 62
- Vlahos, L., Isliker, H., & Lepreti, F. 2004, The Astrophysical Journal, 608, 540
- Werner, G. R., & Uzdensky, D. A. 2017, The Astrophysical Journal Letters, 843, L27
- Yan, H., & Lazarian, A. 2002, Physical review letters, 89, 281102
- Zhdankin, V., Uzdensky, D. A., Werner, G. R., & Begelman, M. C. 2018, Monthly Notices of the Royal Astronomical Society, 474, 2514
- Zhdankin, V., Werner, G. R., Uzdensky, D. A., & Begelman, M. C. 2017, Phys. Rev. Lett., 118, 055103